ACSNANO
www.acsnano.org
ARTICLE

# Self-Assembly of Hierarchical DNA Nanotube Architectures with Well-Defined Geometries

Tyler D. Jorgenson,[†,§] Abdul M. Mohammed,[†] Deepak K. Agrawal,[†] and Rebecca Schulman*[,†,‡]

[†]Chemical and Biomolecular Engineering and [‡]Computer Science, Johns Hopkins University, Baltimore, Maryland 21218, United States

Supporting Information

**ABSTRACT:** An essential motif for the assembly of biological materials such as actin at the scale of hundreds of nanometers and beyond is a network of one-dimensional fibers with well-defined geometry. Here, we demonstrate the programmed organization of DNA filaments into micron-scale architectures where component filaments are oriented at preprogrammed angles. We assemble L-, T-, and Y-shaped DNA origami junctions that nucleate two or three micron length DNA nanotubes at high yields. The angles between the nanotubes mirror the angles between the templates on the junctions, demonstrating that nanoscale structures can control precisely how micron-scale architectures form. The ability to precisely program filament orientation could allow the assembly of complex filament architectures in two and three dimensions, including circuit structures, bundles, and extended materials.

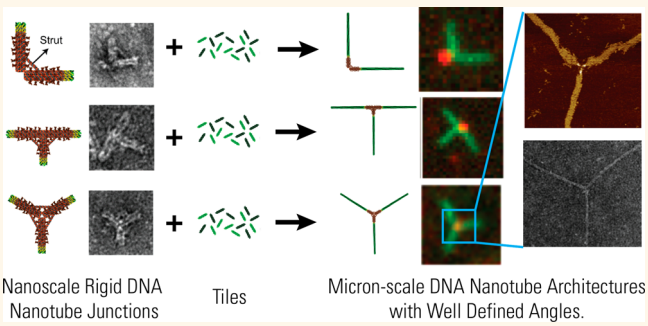


**KEYWORDS:** *DNA nanotechnology, DNA nanotubes, DNA origami, self-assembly, programmable nanostructures, nanotube junctions*

Developing bottom-up fabrication strategies for three-dimensional nanostructures with spatial and orientational control is a central goal of nanotechnology. At the nanometer scale, addressable assembly, where each molecular component, generally a heteropolymer, is used exactly once in the final structure, is a rational design strategy for protein folding or DNA assembly. A variety of such methods exist for controlling the angstrom to nanometer-scale structure of assemblies made from proteins, DNA, RNA, and other heteropolymers[1−10] as well structures in which multiple biomolecular components are assembled hierarchically into extended structures.[11−14] The ability to control the arrangement of matter at these small length scales is critical for controlling functions such as chemical reactivity[15,16] or transport.[17,18]

However, at larger length scales, this design strategy becomes impractical because too many different molecular species are required. Biology suggests how other types of self-assembly processes can address the functional challenges at the micron to millimeter scales. One central organizational motif is the assembly of a single molecular component, a monomer, into many different types of micron-scale structures and architectures. Examples of these processes include the organization of the cytoskeleton, biomineralization, and extracellular matrix.[19−23] Organization of the components of these structures can occur through the use of molecular agents or physical or chemical forces. Within the cytoskeleton, for example, monomers are organized by associating proteins into many different filament architectures. Tubulin, for example, can be organized into cilia, flagella, the spindle, or tracks for cargo transport by molecular motors.[24−26] Because the same monomers are used throughout the assembled structures, relatively few species are required to assemble structures across multiple length scales. Further, the flexibility afforded by this form of organization means that different structures can be formed at different locations in the cell and can be dynamically reorganized over time without the need to resynthesize most of the structural components.

The ability to nucleate the filaments of the cytoskeleton in specific orientations is critical to the formation of higher-order architectures. Proteins such as actin-related protein 2/3 (ARP 2/3) and larger complexes such as a microtubule organizing center[27,28] can direct the nucleation of new filaments at specific orientations to one another or with respect to existing filaments. The resulting junctions, in which semiflexible or rigid filaments are connected at a well-defined angle, form many of the primitives for building the cytoskeleton's large-scale networks or assembled machines.

The ability to design such a dynamic material for organizing biomolecules at the micron scale could make it possible to systematically engineer structures for sensing, transport, and chemical control and to create lightweight materials with

Received: November 29, 2016
Accepted: January 13, 2017
Published: January 13, 2017





DOI: 10.1021/acsnano.6b08008
ACS Nano XXXX, XXX, XXX−XXX

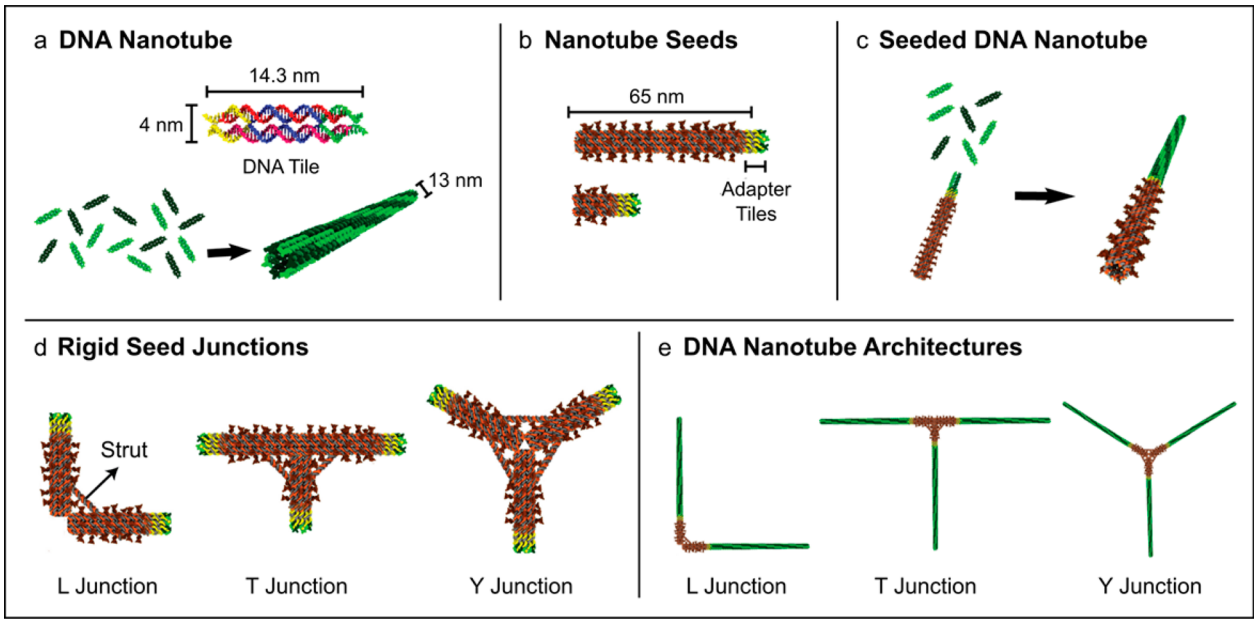


**Figure 1. Schematics of DNA tiles, nanotubes, seeds, and nanotube architectures. (a) DAE-E DNA tiles consist of five DNA strands shown in five different colors. Tiles assemble *via* hybridization of four sticky ends. Two types of tiles with different core and sticky end sequences form a lattice that cyclizes into a DNA nanotube. (b) Structures of the long DNA origami seed consisting of a scaffold (gray) and 72 staple strands (orange) and short DNA origami seed consisting of 24 staple strands. The adapter tiles (yellow) form a facet onto which nanotube tiles can attach. DNA hairpins were presented on the seed exterior to prevent the structure from assembling inside out. Unfolded regions of the M13 scaffold are not shown. (c) Schematic of a seeded DNA nanotube. (d) Design of L, T, and Y seed junctions. (e) Schematic of DNA nanotubes growing from the junctions in (d).**

heterogeneous, adaptive mechanical properties. Various biomolecules have been assembled into nanofibers and nanotubes that range in length from hundreds of nanometers to hundreds of microns.[29−33] Recent advances in structural[17,34] and dynamic[35,36] DNA nanotechnology suggest the possibility that DNA nanostructures and control circuitry might be combined to engineer dynamic filament architectures like those within the cytoskeleton. Specifically, a wide variety of DNA nanotubes with various circumferences, stiffnesses, and assembly mechanisms have been synthesized from small monomer components;[37−41] physical properties of nanotubes such as diffusion and growth rates have been measured,[42−45] and the nucleation of these and related structures may be triggered using a single strand or template.[41,42,46,47] Furthermore, it is possible to control the activity of nanotube monomers or other components using strand displacement cascades or other circuitry.[35] In each of these cases, molecules other than monomers control and determine when and where nanotubes are assembled. However, such control mechanisms only assemble single monomers; they cannot be used to create higher-order two- or three-dimensional architectures.

Here, we show how simple DNA monomers, DAE-E double crossover tiles that form DNA nanotubes[37] (Figure 1a and Supplementary Figure 1), can serve as the substrates for the formation of a variety of micron-scale superstructures containing a precise number of filaments rigidly oriented at designed angles to one another. The same set of simple monomers can form several different structures with a single nucleating complex that serves as a nucleation template and organizer for the component nanotubes directing which structure is assembled. The arrangement of the nucleation sites on the template dictate the resulting arrangement of the filaments that grow from it. Each of the architectures that we study assembles with high yield, and the process requires no purification of assembled components.

The nucleation complexes we assemble are DNA origami structures consisting of (1) motifs that act as nucleation sites, or seeds, for DNA tile nanotube growth and (2) structural components that rigidly organize these nucleation sites at specific angles with respect to one another. The ability to control the structure and orientation of nucleation sites allows us to systematically study how both the structure and organization of nucleation sites affect the nucleation process. We find that changes to the crossover structure of the nucleation site or the sequence of the folded structure have little effect on the high yields of nanotube nucleation, and when nucleation sites are rigidly oriented with respect to one another, the presence of multiple nucleation sites on the same origami scaffold has little effect on the chance of a nanotube nucleating from each site. The modular organization of nucleation sites, in combination with the control over nanoscale structure afforded by the DNA origami design method, thus means that the methods explored here could be extended to form large numbers of junctions, bundles, or other ordered architectures. Further, the assembly of DNA nanotube architectures using filament organizing centers and end-to-end joining of DNA nanotubes[43,45] might together be used to assemble extended materials and networks with well-defined geometries.

Previous work showed that DAE-E DNA tiles composed of five short DNA strands self-assemble into a lattice that cyclizes to form nanotubes (Figure 1a and Supplementary Figure 1). These DNA nanotubes have a precise nanoscale structure that does not appear to have visible warping or twist, even over many microns.[37,43] We have previously shown that a DNA origami seed folded from about 3000 bp of the M13 bacteriophage genome and 96 scaffold strands that presents a facet folded by a set of adapter strands can serve as a template


DOI: 10.1021/acsnano.6b08008
ACS Nano XXXX, XXX, XXX−XXX

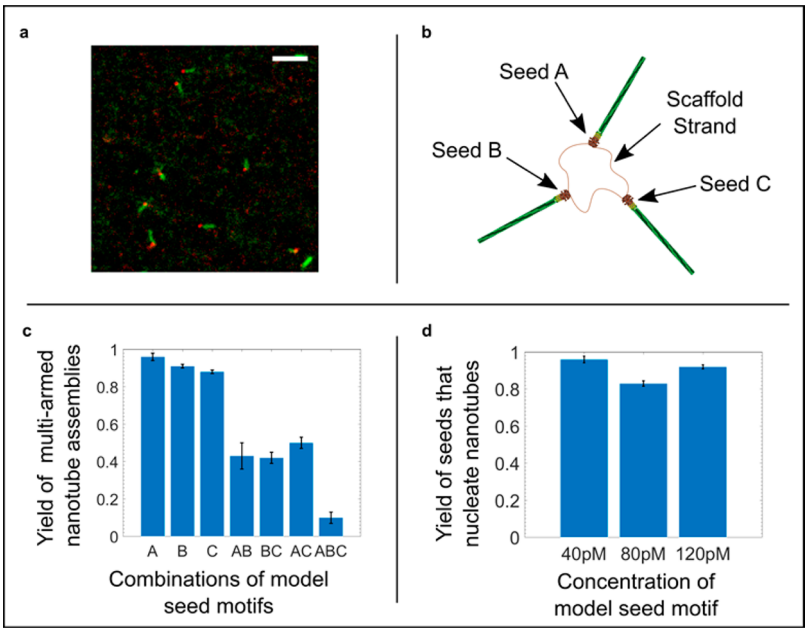


**Figure 2. Nanotubes grow from one or more "model" seed motifs folded on a single M13 scaffold. (a) Fluorescence micrographs of nanotubes (labeled with Cy3) grown from model seed A (labeled with ATTO647N). Scale bar is 5 $\mu$m. (b) Schematic of three model seeds marked A, B, and C on a single M13 scaffold showing nanotubes growing from them. (c) Presenting multiple assembled model seeds on a single scaffold can produce multi-armed nanotube assemblies. Different model seeds (folded from different scaffold regions, Supplementary Figure 3) can have different nucleation yields. (d) Nanotubes grow reliably from model seeds when the seeds are at different seed concentrations (tiles at 40 nM). Error bars here and elsewhere represent one standard deviation.**

for the nucleation of DNA nanotubes[42] (Figure 1b,c). Our goal was to utilize this DNA origami−nanotube system to develop a self-assembly process for self-assembling hierarchical nanotube architectures by building seeds that present multiple templates for nanotube growth with well-defined angles between them (Figure 1d,e).

## RESULTS AND DISCUSSION

In order to build an origami structure using a standard 7−8 kb scaffold strand that presents multiple nucleating facets, we first developed a motif that could nucleate nanotube growth but that uses significantly less than 3000 bp of scaffold used by the long seed. Our goal was that several such small motifs along with rigid components that would orient the position of these motifs could be incorporated within a single 7−8 kb origami design. To develop this motif, we modified the DNA origami seed by removing the staples for the two-thirds of the origami opposite the origami−nanotube facet so that only 1020 bases of the scaffold were folded (Figure 1b and Supplementary Figure 2).

To test how well the short seed motif served as a template for nucleating nanotubes, we compared the fraction of nanotubes that grew from the long and short seeds under identical assembly conditions. We annealed mixtures containing 40 pM M13 scaffold with 16 nM of DNA staples for either the short or long seed, 40 nM of each of the strands for the DAE-E tiles, and 4 nM of adapter strands in standard buffer (see Materials and Methods) from 90 to 32 °C to assemble the seed structure and tiles. The mixture was then incubated for at least 15 h at 32 °C to allow nanotubes to nucleate and grow. Fluorescence microscopy images of aliquots in which nanotubes and seeds were labeled with two different dyes (Supplementary Figure 7) indicated that nanotubes grew from almost all of the long and short seeds: 97.8 ± 0.8% of long seeds had attached nanotubes, whereas 98.4 ± 0.4% of the short seed had attached nanotubes. In addition, 78.4 ± 1.3 and 78.1 ± 2.1% of nanotubes were attached to seeds in the two respective mixtures. These almost identical yield values suggest that short seeds have an almost identical propensity to nucleate nanotubes as the original long seeds.

Next, to test whether multiple nanotubes would grow from multiple nucleation sites presented on a single scaffold, we designed a structure containing three short seed motifs, which we termed model seeds, separated by regions of approximately 1100 bp of unfolded scaffold (Supplementary Figure 3; schematic shown in Figure 2b). The model seeds all have the same crossover structure formed by the staples as the short seed, but each structure is formed from a distinct set of staples, adapter strands, and scaffold regions (see Supplementary Note 2). To determine whether the model seeds could each nucleate nanotubes and could do so whether or not other nucleation sites were presented on the same scaffold, we grew nanotubes using scaffolds where each individual model seed and combinations of two and three model seeds were assembled. Each experiment used the same concentrations of tiles (40 nM) and scaffold (40 pM). During this experiment, we also tested how well nanotube seeds nucleated nanotubes when they were annealed separately from the tiles and then added to a mixture of tiles that had been annealed from 90 to 40 °C; this change allowed us to assemble and if needed purify seeds before assembly. The seeds were heated to 40 °C and then added to the tiles once the tile mixture had also reached 40 °C. The mixture was then cooled to 32 °C and incubated for 15 h to allow nanotubes to grow.

Fluorescence microscopy images showed that nanotubes grew from all the model seeds with reasonable yield, whether the seeds were folded alone on a scaffold or in combination (Figure 2a and Supplementary Figure 8), but the inclusion of multiple templates on the same scaffold lowered the yield of


DOI: 10.1021/acsnano.6b08008
ACS Nano XXXX, XXX, XXX−XXX

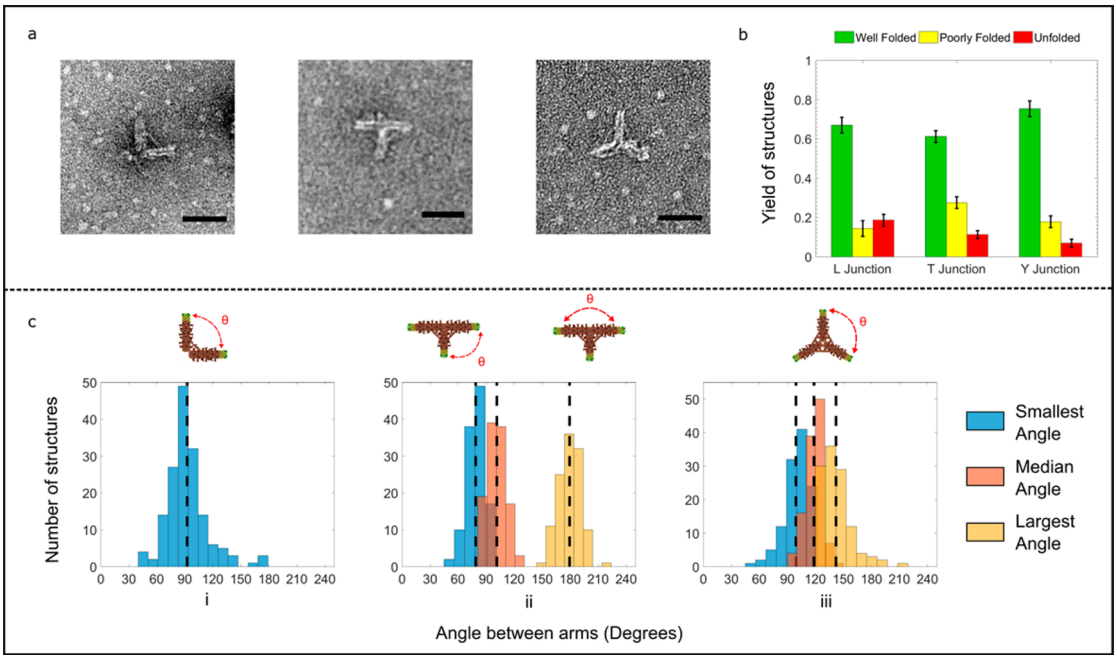


**Figure 3. Structural characterization of DNA origami seed junctions that nucleate DNA nanotube architectures. (a) TEM images of the L (left), T (center), and Y junctions (right). Scale bars are 50 nm. (b) Folding yields of the three junctions determined from AFM images ($N$ = 236, 505, 305, for L, T, and Y, respectively) (see Supplementary Figures 10−12). (c) Distribution of angles between the arms of the seed junctions. Black dashed lines show the mean values of each of the distributions. (i) Distribution of angles between the arms of the L seed junction ($N$ = 160); (ii) distributions of the three angles between the three arms of the T seed junction ($N$ = 116); and (iii) distributions of the three angles between the three arms of the Y seed junction ($N$ = 117).**

growth from each individual template when compared with yields when only one template was present (Figure 2c). The fraction of individual model seeds that grew nanotubes were 96 ± 2, 91 ± 1, and 88 ± 1% for the three seed structures. If the probability that a given seed would nucleate a nanotube was independent of whether the other seeds were present and nanotubes grew from them, we would expect 77 ± 3% of structures to nucleate three nanotubes. However, in experiments in which all seeds were assembled simultaneously, just 14 ± 3% of structures observed presented three growing nanotubes.

We considered several potential explanations for the low yields observed. Such decreases in yield could occur if the templates interacted with one another, so that some template sites were unavailable for growth some or all of the time. Depletion effects that caused tiles to attach to an already growing nanotube rather than a bare template could also be responsible, although, as we will describe, depletion does not seem to occur in other experiments when multiple nucleation is present in a small area. Finally, the inclusion of multiple templates on the same scaffold increases the template concentration. This increase in concentration may decrease yields of growth from each template because a larger number of templates more quickly deplete tiles, and as there is a small nucleation barrier to growth from each template, the rate of initiating nanotube growth from a template decreases with decreasing tile concentration.[42] Together, these effects could limit the amount of time during which a nanotube is able to grow readily from a given nucleation site. To test the extent to which yields would decrease with increasing template concentration, we grew nanotubes from a single model seed at scaffold concentrations of 40, 80, and 120 pM (Figure 2d). There was a slight decrease in yield as template concentration increased, but not enough to explain the decreased yield observed when templates were presented in combination on the same scaffold.

Alternatively, the low yields observed may have to do with the flexible nature of the scaffold. Nanotubes nucleated from the model seeds can rotate so that they overlap on micrographs. If two nanotubes overlapped (or were joined at their sides), such structures might appear to have only two nanotubes growing from three model seeds. Another possibility is that the flexible scaffold allows the templates to interact with each other such that they cannot bind tiles and nucleate nanotubes.

In order to build structures where nanotubes are oriented with respect to one another at specific angles, we designed three DNA origami structures that presented multiple sites for nucleating nanotubes: an L, T, and Y (Figure 1d). The T junction was composed of an original seed motif with nucleating sites at each edge and a shorter seed motif, which consisted of three rows of staples, longer than the two rows of staples used for the short seed and shorter than the six rows of staples in the original seed motif. The L and Y junctions were composed of only the shorter seed motifs. These lengths ensured that most of the scaffold was folded as part of the structures. To arrange the seed motifs into rigid multidomain structures, we used double-stranded DNA struts whose lengths dictate the angles between seed arms. This approach was inspired by early work[7,14] in which struts were used to connect honeycomb lattice components. Because the components connected in our structures are hollow cylinders, it was important to choose the locations where struts are placed carefully, as CanDo simulations[48] of the folded structures indicated that struts could deform the overall structure. To ensure that the structure was rigid and entirely folded, we also introduced new crossover points and removed crossover points



DOI: 10.1021/acsnano.6b08008
ACS Nano XXXX, XXX, XXX−XXX

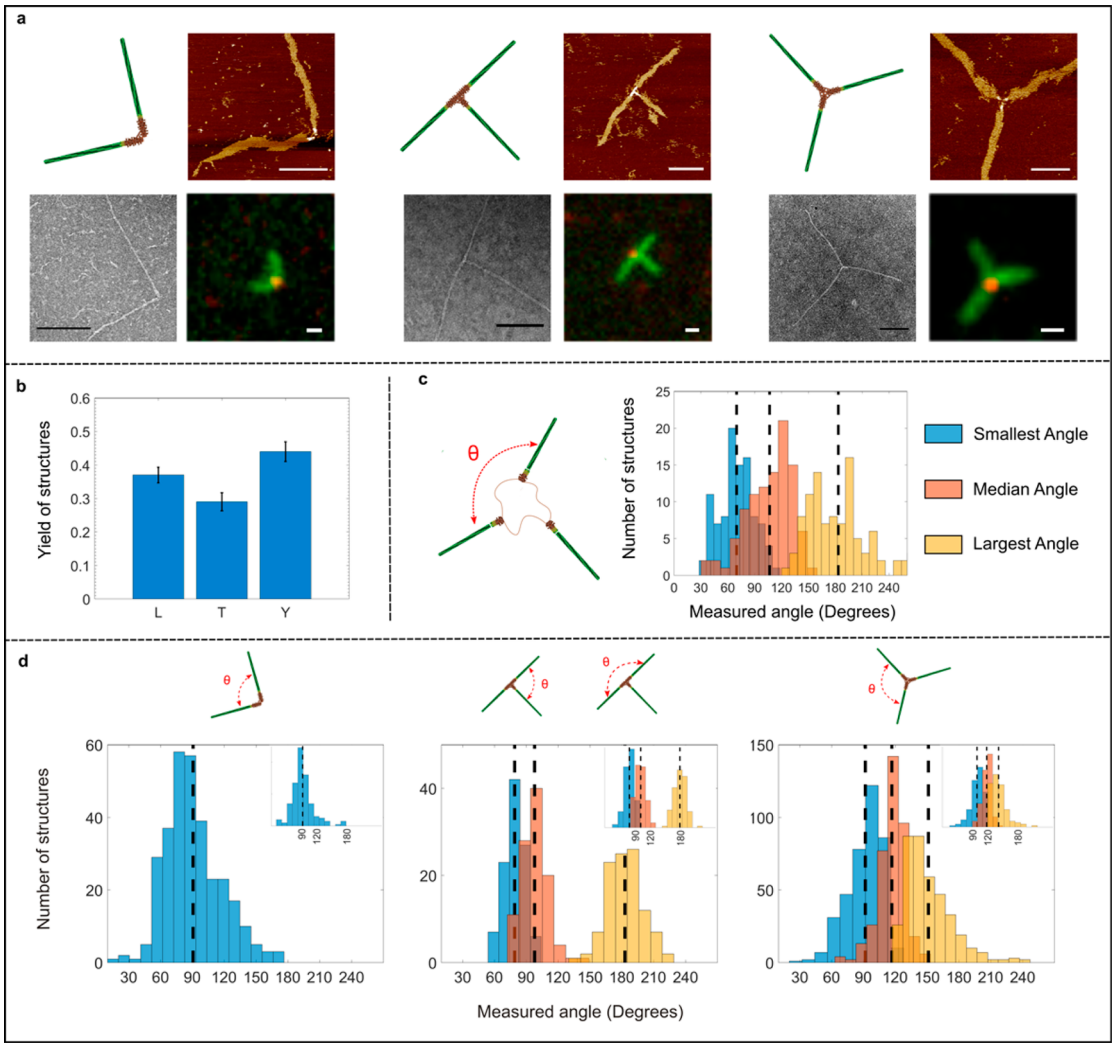


**Figure 4. Seed-junction-templated DNA nanotube architectures. (a) Expected nanotube architecture structure and clockwise from top left, atomic force, transmission electron, and fluorescence micrographs of assembled architectures. AFM and TEM scale bars are 250 nm; fluorescence micrograph scale bar is 1 μm. The AFM images show mica-surface-mediated opening of nanotubes.[37] (b) Nanotube architecture yields. Error bars are one standard deviation ($N$ = 777, 586, and 566 for the L, T, and Y, respectively). (c) Schematic of three model seeds on a single M13 scaffold and distributions of the smallest, median, and largest angles measured between the nanotubes grown from the seeds. Black dashed lines show distribution means. (d) Distributions of the smallest, median, and largest angles between the nanotubes within L, T and Y nanotube architectures. Black dashed lines show distribution means. (i) L junction ($N$ = 313). (ii) T junction ($N$ = 105). (iii) Y junction ($N$ = 384). The inset graphs show the angle distributions from Figure 3c for the respective seed junction.**

to account for the addition of the struts. In addition to the strut connections, DNA helices on adjacent seeds connected by the struts were also attached by 10 bp of single-stranded scaffold that connect the seeds at the bases of their respective cylinders, forming a vertex between the seed motifs (Supplementary Figures 4–6).

To self-assemble the seed junctions with high yields, we developed an annealing protocol for the L structure based on previous methods developed by Sobszak *et al.*,[49] in which the majority of the folding time was spent at the temperature where the greatest amount of folding was observed during a slow, initial anneal (Supplementary Figure 9 and Supplementary Note 3). We used this protocol to fold each of the seed junctions (see Materials and Methods).

Transmission electron microscopy (TEM) images showed that each of the seed junctions formed as designed (Figure 3a). Atomic force microscopy (AFM) images showed that 63 ± 4, 61 ± 3, and 75 ± 4% of the L, T, and Y junctions, respectively, were well-folded (Figure 3b and Supplementary Figures 10–12). In AFM images, the short regions of the L and Y junctions were 34 ± 1 and 34 ± 1 nm, respectively, and the length of the short seed leg in the T junction was 29 ± 1 nm, close to the predicted lengths (assuming each base pair of double-stranded DNA contributed 0.33 nm to the total length) of 32 nm for the short seed. The long axis of the T junction was 69 ± 1 nm, which also corresponds well with the predicted length of 66 nm.

To determine whether the angles between the junction arms matched the designed angles, we used TEM images because they provided better resolution than AFM images (Supplementary Figures 13–18 and Supplementary Notes 5 and 6). The L junction angle is designed to be 90° and was measured as 92 ± 22° ($N$ = 160, Figure 3c). The large standard deviation may reflects the inclusion of some outliers with very large angles that likely did not form correctly.



DOI: 10.1021/acsnano.6b08008
ACS Nano XXXX, XXX, XXX–XXX

The T junction was designed to have two 90° angles and one 180° angle, whereas the Y junction was designed to have three identical 120° angles. To characterize how close the sizes of the three angles between arms of the T and Y junctions were to the designed angle sizes, we compared the sizes of the smallest, median, and largest angles of the junctions. The smallest, median, and largest angles between the arms of the T junction were 79 ± 9, 102 ± 10, and 180 ± 12° and between the arms of the Y junction were 99 ± 12, 119 ± 10, and 142 ± 16° (Figure 3c).

Previous work that used struts to control the orientation of two origami lattice plates reported standard deviations on the order of 5°, about three times smaller than what we observed. However, twice as many struts were incorporated between the plates of those structures than between the arms of the seed junctions, and the struts were no more than 50 bp, about half the length of the struts within the seed junctions. Shorter struts presumably result in a smaller degree of thermal fluctuations.[7] The range of angles observed here is thus qualitatively consistent with other work and could also potentially be improved by increasing the number of struts.

To form nanotube architectures using origami seed junctions, we first annealed each of the origami junctions and added them without purification to a tile solution (see Materials and Methods). We characterized the resulting nanotube architectures using atomic force, fluorescence, and transmission electron microscopy (Figure 4a and Supplementary Figures 19−28). The percentages of L, T, and Y nanotube architectures that displayed the expected number of nanotube arms were 37 ± 2, 29 ± 3, and 45 ± 3%, respectively. In each case, nanotube nucleation yields significantly exceeded the nucleation yield of nanotube architectures grown from the three model seeds. Least-squares analysis of the number of structures presenting different number of arms suggested that 59 ± 2% of the nucleation sites on the L junctions, 65 ± 1% of the nucleation sites on the T junctions, and 77 ± 1% of the nucleation sites on the Y templates grew nanotubes (Supplementary Note 8). These yields are significantly lower than the nanotube nucleation yields from the individual long and short seeds, presumably at least in part because, in many structures, all of the templates were not well formed. The least-squares analysis also suggested that the nanotube arms of the T and Y nucleated with probabilities that were nearly independent of one another, but that whether one nanotube arm of the L nucleates may be slightly dependent on whether the other nanotube arm nucleates (Supplementary Figure 29). Overall, however, the growth of each of the nanotubes from the arms of the seed junction appears to occur independently of the other arms. Thus, rigidly orienting seeds so that they cannot interact appears to enable nucleation of the various nanotube arms to proceed essentially independently of one another.

Our least-squares analysis assumed that the probabilities of nucleation at each site on a seed junction were the same. We tested this assumption by growing nanotubes from Y junctions where only one or combinations of the three sets of seed staple strands were present so that only some of the templates could assemble. The yields of nanotubes grown from each of the three arms of the Y junction presented one at a time were 81 ± 2, 88 ± 1, and 84 ± 3%, confirming this assumption. The percentages of two armed structures that grew two nanotubes were nearly indistinguishable from each other ranging from 65 ± 4 to 70 ± 3%. Pooling yield data from these experiments with the growth of the full Y structure produced a least-squares fit of nucleation rates for the three seed motifs of 80 ± 4, 85 ± 4, and 78 ± 4%. Taken together, these results suggest that the changes made to the crossover structure and staple sequences of the nucleation sites had negligible effects on nucleation yields.

The seed junctions were designed to present nucleation sites at well-defined angles with the idea that the angle between the nanotubes that grow at the nucleation sites should mirror the angle between the nucleation sites. To characterize the effectiveness of this mechanism for controlling nanotube orientation, we measured the angles between the nanotubes within assembled architectures and compared them to the angles measured between the arms of the seed junctions that nucleated the architectures. To understand what angles between nanotubes that would be observed if no rigid junction controlled the relative orientations of the nanotubes, we first measured the angles between nanotubes within an architecture where the nucleation sites were connected only by a flexible single-stranded scaffold. We grew nanotube architectures from the three model seeds as well as a modified Y junction in which only the staples for the short seed motifs (but not the connecting struts) were included. For the architectures assembled by three model seeds, the smallest, median, and largest angles were 70 ± 19, 107 ± 25, and 183 ± 35° (Figure 4c). The angles between the nanotubes in architectures assembled by the modified Y junction were virtually identical: the smallest, median, and largest angles were 72 ± 19, 109 ± 23, and 173 ± 33°, respectively. These angles were similar to those that would be observed between three vectors emanating from the origin placed at random orientations (Supplementary Note 9).

In contrast, nanotubes grown from rigid seed junctions displayed a clear preference for angular orientations that reflected the angles at which their growth templates were presented (Figure 4d). The average angle between the nanotube arms of the L architecture was 91 ± 27°, virtually identical to the angles between the arms of the L seed structure. When considering only angles between 60 and 120°, the average angle between nanotube arms becomes 87 ± 15°. In both of these cases, the standard deviation of the angles for the architectures is similar to the standard deviations found in the analogous distributions of the L junction arms in TEM micrographs (22 and 13°, respectively), suggesting that not only is the average angle between nanotubes controlled by the seed junction, but the standard deviations, or variations about this angle for the nanotube architecture, are largely controlled by the variations in the angles of the nanotube seed junction, as well. This observation suggests that the nucleation template rigidly and specifically aligns the nanotube with the facet on the junction without any distortion or bending of the seed structure, and that the variations in angles that are observed between nanotubes are largely the variations in the angles between the arms of the seed junction. It is further interesting to note that the fraction of "outlier" architectures, with angles between the nanotubes outside of the 60−120° range we considered, is similar to the fraction of L junctions with structures positioned outside this angle. These "outliers" may be structures in which the strut was malformed or unfolded (see Supplementary Figure 14).

The mean angles between the nanotubes grown from the T and Y seeds were likewise very similar to the mean angles between the arms of the T and Y junctions. The average of the largest angle between nanotubes in the T structure was 183 ± 17°, with the smaller and larger of the two remaining angles


DOI: 10.1021/acsnano.6b08008
ACS Nano XXXX, XXX, XXX−XXX

measuring 79 ± 9 and 98 ± 12°, respectively. The average sizes of the smallest, median, and largest angles between the nanotubes grown from the Y junction were 92 ± 17, 117 ± 13, and 151 ± 22°, respectively. Just as there tended to be two smaller and one slightly larger angle between the arms of the Y junction, there were also two smaller and one slightly larger angle between the nanotubes in the Y-junction-nucleated nanotube architecture. Together, these results show how the nanoscale origami seeds can precisely control the structure of the micron-scale nanotube architectures grown from them.

A potential advantage of assembling architectures by nucleating nanotubes rather than assembling existing nanotubes is that control exerted over the assembly process should also provide some control over nanotube length because nanotubes begin growing at approximately the same time and can increase in length through monomer addition at similar rates.[42,50] In contrast, nanotubes nucleated heterogeneously would be expected to have lengths that are exponentially distributed, which leads to high polydispersity. The average length of nanotubes nucleated from the L, T, and Y junctions were 1.13 ± 0.30, 1.04 ± 0.27, and 1.14 ± 0.30 μm, respectively (Supplementary Figure 30). The nanotube length distributions were each peaked and fairly symmetric about the mean length with slight positive skews (Supplementary Figure 30), consistent with assembly through nucleation at the seed and growth at a relatively constant rate through monomer addition[42,51] rather than through repeated nanotube nucleation and joining.[43] Such a mechanism for the assembly of nanotubes within architectures is consistent with the assembly of dynamic structures that can grow in response to the addition of new monomers over time or begin growing as the nucleation sites are assembled.[34,52]

Qualitative evaluation of fluorescence micrographs of nanotube architectures suggested that nanotubes nucleated from the same seed junction had similar lengths. In order to quantify this similarity, we measured the length of each nanotube nucleated from the same seed junction. The coefficient of variation of nanotube lengths within individual L, T, and Y junctions was 22, 22, and 23%, respectively, whereas the coefficient of variation between all nanotube lengths was 26% for each seed junction, suggesting that nanotubes within a single architecture may be slightly more similar than the population as a whole.

## CONCLUSIONS

In this paper, we have developed a method to build self-assembled, micron-scale DNA nanotube architectures in which the number of nanotubes within the architecture and the angle between them are precisely controlled. To do so, we developed a simple modular DNA nanostructure motif that nucleates a DNA nanotube with high yield. Such multiple motifs can be folded from different portions of a single DNA scaffold, either connected by flexible linkers or arranged at well-defined angles with respect to one another. The resulting seed junctions can nucleate nanotubes at each of the seed motifs at high yields, forming nanotube architectures where the valence and relative orientations of the component nanotube are precisely controlled by the nucleation template.

Seed junction domains may be assembled as modules and arranged into rigid geometries using a set of programmable struts, suggesting a straightforward route to assembling a combinatorial variety of two- or three-dimensional branched architectures. Other DNA origami techniques suggest routes to the assembly of bundles similar to the axoneme structure of microtubules[53] or other nanotube architectures. Nanotubes with different sequences or radii[42] could also be assembled into heterogeneous structures, and the assembly process could be extended to allow for stepwise or hierarchical assembly to produce structures with more than one junction to create extended materials. Combined with the array of site-specific modification methods available for DNA nanotubes and seed junctions,[54,55] such an ability to control material structure across the nanometer to micron size scales is of fundamental interest for diverse problems such as plasmonic device design,[56] biomaterials synthesis,[57,58] and membrane design.[59,60]

The nucleation of DNA nanotubes from origami templates could also be used as a means for readout of the template structure. The average angle between the nanotubes that grow from the architectures we have synthesized is the same as the average angle between the templates on the origami structure, so imaging the angle between nanotubes could be used to deduce the angles of nucleation templates added to other origami nanostructures. Further, because nanotube dynamics can be readily tracked in free solution,[51] such a method could allow nanoscale motion or fluctuations of DNA nanostructures to be measured over time using standard fluorescence microscopy techniques.

Finally, recent developments have shown how DNA nanotube assembly and disassembly can be triggered by strand displacement methods.[35] DNA nanostructures may be fragmented by extensional flows[45,61,62] and could serve as tracks for DNA-based molecular motors[63] that modify their structure.[63] Such behaviors can be precisely programmed and observed *in situ* using methods such as time-lapse fluorescence microscopy or high-speed AFM. The advances described here mean that these mechanisms could be used to assemble or alter the structure of not only one-dimensional filaments but also DNA nanotube architectures. The ability to program complex dynamic responses to a diverse array of chemical and physical inputs suggests a way in which, as the cytoskeleton vividly illustrates, simple chemical primitives may be organized into a diverse array of micron-scale assemblies, materials, and machines.

## MATERIALS AND METHODS

**Design and Self-Assembly of DNA Origami Seeds and Seed Junctions.** Sequences for DNA origami structures were designed using Cadnano 2.[8] Integrated DNA Technologies, Inc. (IDT) synthesized all DNA strands used in this study except the M13mp18 scaffold strand, which was purchased from Bayou Biolabs. To form the origami seed junctions, we annealed solutions of 10 nM M13 scaffold strand containing 100 nM of each DNA staple strand in 40 mM Tris-acetate and 1 mM EDTA buffer containing 12.5 mM magnesium acetate (TAE $Mg^{2+}$ buffer). The solution was heated to 65 °C for 15 min and then immediately dropped to 47 °C for 48 h, after which the temperature was decreased by 1 °C per minute until the thermocycler reached room temperature. The annealing schedule was developed using methods from Sobczak *et al.*[49] applied to the L junction (see Supplementary Note 3).

**Self-Assembly of DNA Nanotubes.** The DNA nanotube tile and adapter strands were PAGE purified by IDT, while Cy3 and ATTO647N fluorophore strands were HPLC purified. Stock solution concentrations of DNA tile and adapter strands were determined using 260 nm absorbance measurements and extinction coefficients provided by IDT. Staple strands were not purified after synthesis and were used as stock solutions at concentrations specified by IDT (Supplementary Note 1). To grow nanotube architectures, we first annealed the origami seed junctions as described above except that 100 nM of each


DOI: 10.1021/acsnano.6b08008
ACS Nano XXXX, XXX, XXX−XXX

adapter strand was also included in the assembly mixture. Next, a mixture containing 40 nM DNA tiles, 4 nM adapter strands, and TAE $Mg^{2+}$ (standard) buffer was annealed from 90 to 45 °C at 1 °C per minute, held at 45 °C for 1 h, and then annealed from 45 to 32 °C at 0.1 °C per minute. Additional adapter strands were included in the nanotube assembly mixture as we previously found that the presence of additional adapters improved yields of nanotube nucleation from seeds potentially due to attachment of additional adapters to empty adapter binding sites.[64] Once the tile mixture reached 40 °C, preannealed origami seed junctions were heated to 40 °C and then added to the mixture at a final concentration of 40 pM of scaffold. Samples were incubated at 32 °C for at least 15 h to allow nanotubes to nucleate and grow. For fluorescence microscopy experiments, 0.6 nM of ATTO647N attachment strands and 35 nM of ATTO647N-labeled DNA strands were added to the mixture in order to track seeds and seed junctions (Supplementary Figure 7).

**AFM Imaging.** Imaging was preformed on a Dimension Icon (Bruker) using Scanasyst mode and sharp nitride lever tip (SNL-10 C, Bruker) cantilevers. Images were flattened based upon a linear fit using Nanoscope Analysis software. To image seed junctions, 2 μL of an annealed solution containing 10 nM seed junctions was added to freshly cleaved mica surfaces mounted on a puck with a Teflon sheet. To image DNA nanotube architectures, 20 μL of annealed samples at 0.08 nM was added to the mica surfaces after incubation with 2 μL of 4 μM guard strands that prevent further nanotube growth by deactivating free tiles and nanotube facets[42] (Supplementary Note 10). All samples were incubated on the mica surface for 30 s before being washed once with approximately 100 μL of standard buffer. Imaging was performed in solution. The length of the seed was taken to be the width measured at half of the maximum height of the AFM height section profile.

**Fluorescence Microscopy.** Fluorescence microscopy experiments were performed after the assembly mixtures for nanotube architectures were annealed and then incubated for at least 15 h. To prevent growth of nanotubes after they were cooled from the incubation temperature of 32 °C to room temperature, we added 5 μL of 4 μM guard strands, which bound to tiles and prevented further interaction, to 50 μL of 40 nM of nanotube architecture solution and then incubated for 1 min[42] (Supplementary Note 10). Six microliters of the assembly mixture was pipetted onto a coverslip, placed onto a slide, and the edges of the coverslip were sealed with wax. The samples were imaged on an inverted microscope (Olympus IX71) using a 60×/1.45 NA oil immersion objective, and images were taken using the Cy3 and ATTO647N filters and then overlaid to produce two-color images. Images were captured on a cooled CCD camera (iXON3, Andor).

**Transmission Electron Microscopy and Grid Preparation.** Before imaging, carbon-coated Cu400 TEM grids were glow discharged for 30 s. The discharged grids were then treated with 0.5 M magnesium acetate for 2 min. Then, either 10 μL of 1 nM annealed seeds or 10 μL of a nanotube architecture solution with 80 pM of seed junctions was adsorbed for 10 or 25 min, respectively. The grids were then stained for 30 s with 10 μL of 2% uranyl formate solution containing 25 mM of sodium hydroxide (Supplementary Note 4). After each step, excess liquid was removed using the torn edge of a piece of filter paper. The grids were air-dried. Imaging was performed on a FEI Tecnai 12 operated at 100 kV.

## ASSOCIATED CONTENT

### Supporting Information

The Supporting Information is available free of charge on the ACS Publications website at DOI: 10.1021/acsnano.6b08008.

Sequences for oligonucleotides used in our experiments, schematics for DNA origami designs, additional experimental data, and all notes referred to in this paper (PDF)

## AUTHOR INFORMATION


### Corresponding Author

*E-mail: rschulm3@jhu.edu.

### ORCID

Rebecca Schulman: 0000-0003-4555-3162

### Present Address

§Molecular Engineering and Sciences Institute, University of Washington, Seattle, WA 98105.


### Author Contributions

T.D.J., A.M.M., D.K.A., and R.S. designed the experiments and did the experimental analysis. T.D.J. and A.M.M. conducted the experiments. All the authors discussed the results, and T.D.J. and R.S. wrote the manuscript.

### Notes

The authors declare no competing financial interest.

## ACKNOWLEDGMENTS

The authors would like to thank D. Fygenson and Seth Reinhart for helpful discussions and advice on the manuscript, and Dr. Michael McCaffery for providing the necessary technical training for using the TEM. This research was primarily supported by DOE Grant DE-SC0010595, which supported T.D.J. and D.K.A. and provided most materials and supplies. A.M.M. was supported by NSF CAREER Award 125387. Material support was also provided by a JHU Provost's Undergraduate Research Award to T.D.J.

## REFERENCES


(1) Rothemund, P. W. K. Folding DNA to Create Nanoscale Shapes and Patterns. *Nature* **2006**, *440*, 297−302.

(2) Geary, C.; Rothemund, P. W. K.; Andersen, E. S. A Single-Stranded Architecture for Cotranscriptional Folding of RNA Nanostructures. *Science* **2014**, *345*, 799−804.

(3) Han, D.; Suchetan, P.; Liu, Y.; Yan, H. Folding and Cutting DNA into Reconfigurable Topological Nanostructures. *Nat. Nanotechnol.* **2010**, *5*, 712−717.

(4) Howorka, S. Rationally Engineering Natural Protein Assemblies in Nanobiotechnology. *Curr. Opin. Biotechnol.* **2011**, *22*, 485−491.

(5) Ke, Y.; Ong, L. L.; Shih, W. M.; Yin, P. Three-Dimensional Structures Self-Assembled from DNA Bricks. *Science* **2012**, *338*, 1177−1183.

(6) Dietz, H.; Douglas, S.; Shih, W. M. Folding DNA into Twisted and Curved Nanoscale Shapes. *Science* **2009**, *325*, 725.

(7) Funke, J. J.; Dietz, H. Placing Molecules with Bohr Radius Resolution using DNA Origami. *Nat. Nanotechnol.* **2016**, *11*, 47−52.

(8) Douglas, S. M.; Marblestone, A. H.; Teerapittayanon, S.; Vazquez, A.; Church, G. M.; Shih, W. M. Rapid Prototyping of 3D DNA-Origami Shapes with CaDNAno. *Nucleic Acids Res.* **2009**, *37*, 5001−5006.

(9) Zhang, F.; Jiang, S.; Wu, S.; Li, Y.; Mao, C.; Liu, Y.; Yan, H. Complex Wireframe DNA Origami Nanostructures with Multi-Arm Junction Vertices. *Nat. Nanotechnol.* **2015**, *10*, 779−784.

(10) Pinheiro, A.; Han, D.; Shih, W. M.; Yan, H. Challenges and Opportunities for Structural DNA Nanotechnology. *Nat. Nanotechnol.* **2011**, *6*, 763−772.

(11) Zhao, Z.; Liu, Y.; Yan, H. Organizing DNA Origami Tiles into Larger Structures Using Preformed Scaffold Frames. *Nano Lett.* **2011**, *11*, 2997−3002.

(12) Fern, J.; Lu, J.; Schulman, R. The Energy Landscape for the Self-Assembly of a Two-Dimensional DNA Origami Complex. *ACS Nano* **2016**, *10*, 1836−1844.

(13) Zenk, J.; Tuntivate, C.; Schulman, R. Kinetics and Thermodynamics of Watson-Crick Base Pairing Driven DNA Origami Dimerization. *J. Am. Chem. Soc.* **2016**, *138*, 3346−3354.

(14) Iinuma, R.; Ke, Y.; Jungmann, R.; Schlichthaerle, T.; Woehrstein, J. B.; Yin, P. Polydhedra Self-Assmbled from DNA Tripods and Characterized with 3D DNA-PAINT. *Science* **2014**, *344*, 65−69.
(15) Simmel, F. DNA-Based Assembly Lines and Nanofactories. *Curr. Opin. Biotechnol.* **2012**, *23*, 516−521.
(16) Li, X.; Liu, D. R. DNA-Templated Organic Synthesis: Nature's Strategy for Controlling Chemical Reactivity Applied to Synthetic Molecules. *Angew. Chem., Int. Ed.* **2004**, *43*, 4848−4870.
(17) Burns, J.; Seifert, A.; Fertig, N.; Howorka, S. A Biomimetic DNA-Based Channel for the Ligand-Controlled Transport of Charged Molecular Cargo Across a Biological Membrane. *Nat. Nanotechnol.* **2016**, *11*, 152−156.
(18) Bell, N. A. W.; Engst, C. R.; Ablay, M.; Divitini, G.; Ducati, C.; Liedl, T.; Keyser, U. F. DNA Origami Nanopores. *Nano Lett.* **2012**, *12*, 512−517.
(19) Daley, W. P.; Peters, S. B.; Larsen, M. Extracellular Matrix Dynamics in Development and Regerative Medicine. *J. Cell Sci.* **2008**, *121*, 255−264.
(20) De Yoreo, J. J.; Vekilov, P. G. Principles of Crystal Nucleation and Growth. *Rev. Mineral. Geochem.* **2003**, *54*, 57−93.
(21) Fletcher, D. A.; Mullins, R. D. Cell Mechanics and the Cytoskeleton. *Nature* **2010**, *463*, 485−492.
(22) Vignaud, T.; Blanchoin, L.; Thery, M. Directed Cytoskeleton Self-Organization. *Trends Cell Biol.* **2012**, *22*, 671−682.
(23) Singh, P.; Carraher, C.; Schwarzbauer, J. E. Assembly of Fibronectin Extracellular Matrix. *Annu. Rev. Cell Dev. Biol.* **2010**, *26*, 397−419.
(24) Mohri, H.; Inaba, K.; Ishijima, S.; Baba, S. Tubulin-Dynein System in Flagellar and Ciliary Movement. *Proc. Jpn. Acad., Ser. B* **2012**, *88*, 397−415.
(25) Hirokawa, N. Kinesin and Dynein Superfamily Proteins and the Mechanism of Organelle Transport. *Science* **1998**, *279*, 519−526.
(26) Nogales, E.; Wolf, S.; Downing, K. Structure of the Alpha-Beta-Tubulin Dimer by Electron Crystallography. *Nature* **1997**, *391*, 199−203.
(27) Luders, J.; Stearns, T. Micotubule-Organizing Centers: A Re-Evaluation. *Nat. Rev. Mol. Cell Biol.* **2007**, *8*, 161−167.
(28) Campellone, K. G.; Welch, M. D. A Nucleator Arms Race: Cellular Control of Actin Assembly. *Nat. Rev. Mol. Cell Biol.* **2010**, *11*, 237−251.
(29) Douglas, S.; Chou, J.; Shih, W. DNA-Nanotube-Induced Alignment of Membrane Proteins for NMR Structure Determination. *Proc. Natl. Acad. Sci. U. S. A.* **2007**, *104*, 6644−6648.
(30) Gao, X.; Matsui, H. Peptide-Based Nanotubes and Their Applications in Bionanotechnology. *Adv. Mater.* **2005**, *17*, 2037−2050.
(31) Hartgerink, J. D.; Beniash, E.; Stupp, S. Self-Assembly and Mineralization of Peptide-Amphiphile Nanofibers. *Science* **2001**, *294*, 1684−1688.
(32) Zhang, S. Fabrication of Novel Biomaterials Through Molecular Self-Assembly. *Nat. Biotechnol.* **2003**, *21*, 1171−1178.
(33) Morikawa, M.; Yoshihara, M.; Endo, T.; Kimizuka, N. ATP as Building Blocks for the Self-Assembly of Excitonic Nanowires. *J. Am. Chem. Soc.* **2005**, *127*, 1358−1359.
(34) Marras, A.; Zhou, L.; Su, H.; Castro, C. Programmable Motion of DNA Origami Mechanisms. *Proc. Natl. Acad. Sci. U. S. A.* **2014**, *112*, 713−718.
(35) Zhang, D.; Hariadi, R. F.; Choi, H.; Winfree, E. Integrating DNA Strand-Displacement Circuitry with DNA Tile Self-Assembly. *Nat. Commun.* **2013**, *4*, 1965.
(36) Zhang, D.; Seelig, G. Dynamic DNA Nanotechnology Using Strand-Displacement Reactions. *Nat. Chem.* **2011**, *3*, 103−113.
(37) Rothemund, P. W. K.; Ekani-Nkodo, A.; Papadakis, N.; Kumar, A.; Fygenson, D. K.; Winfree, E. Design and Characterization of Programmable DNA Nanotubes. *J. Am. Chem. Soc.* **2004**, *126*, 16344−16352.
(38) Aldaye, F.; Lo, P.; Karam, P.; McLaughlin, C.; Cosa, G.; Sleiman, H. Modular Construction of DNA Nanotubes of Tunable Geometry and Single- or Double-Stranded Character. *Nat. Nanotechnol.* **2009**, *4*, 349−352.
(39) Hou, S.; Wang, J.; Martin, C. Template-Synthesized DNA Nanotubes. *J. Am. Chem. Soc.* **2005**, *127*, 8586−8587.
(40) Yin, P.; Hariadi, R. F.; Sahu, S.; Choi, H.; Park, S.; LaBean, T.; Reif, J. Programming DNA Tube Circumferences. *Science* **2008**, *321*, 824−826.
(41) Wilner, O.; Orbach, R.; Henning, A.; Teller, C.; Yehezkeli, O.; Mertig, M.; Harries, D.; Willner, I. Self-Assembly of DNA Nanotubes with Controllable Diameters. *Nat. Commun.* **2011**, *2*, 540.
(42) Mohammed, A. M.; Schulman, R. Directing Self-Assembly of DNA Nanotubes Using Programmable Seeds. *Nano Lett.* **2013**, *13*, 4006−4013.
(43) Ekani-Nkodo, A.; Kumar, A.; Fygenson, D. K. Joining and Scission in the Self-Assembly of Nanotubes from DNA Tiles. *Phys. Rev. Lett.* **2004**, *93*, 268301.
(44) Hariadi, R. F.; Yurke, B.; Winfree, E. Thermodynamics and Kinetics of DNA Nanotube Polymerization from Single-Filament Measurements. *Chem. Sci.* **2015**, *6*, 2252−2267.
(45) Hariadi, R. F.; Winfree, E.; Yurke, B. Determining Hydrodynamic Forces in Bursting Bubbles using DNA Nanotube Mechanics. *Proc. Natl. Acad. Sci. U. S. A.* **2015**, *112*, E6086−E6095.
(46) Barish, R. D.; Schulman, R.; Rothemund, P. W. K.; Winfree, E. An Information-Bearing Seed for Nulceating Algorithmic Self-Assembly. *Proc. Natl. Acad. Sci. U. S. A.* **2009**, *106*, 6054−6059.
(47) Lau, K.; Sleiman, H. Minimalist Approach to Complexity: Templating the Assembly of DNA Tile Structures with Sequentially Grwon Input Strands. *ACS Nano* **2016**, *10*, 6542−6551.
(48) Kim, D.-N.; Kilchherr, F.; Dietz, H.; Bathe, M. Quantitative Prediction of 3D Solution Shape and Flexibility of Nucleic Acid Nanostructures. *Nucleic Acids Res.* **2012**, *40*, 2862−2868.
(49) Sobczak, J.-P. J.; Martin, T. G.; Dietz, H. Rapid Folding of DNA into Nanoscale Shapes at Constant Temperature. *Science* **2012**, *338*, 1458−1461.
(50) Flory, P. *Principles of Polymer Chemistry*; Cornell University Press: Ithaca, NY, 1953; Vol. *17*.
(51) Mohammed, A. M.; Šulc, P.; Zenk, J.; Schulman, R. Self-Assembling DNA Nanotubes to Connect Molecular Landmarks. *Nat. Nanotechnol.* **2016**, DOI: 10.1038/nnano.2016.277.
(52) Tikhomirov, G.; Petersen, P.; Qian, L. Programmable Disorder in Random DNA Tilings. *Nat. Nanotechnol.* **2016**, DOI: 10.1038/nnano.2016.256.
(53) Nicastro, D.; Schwartz, C.; Pierson, J.; Gaudette, R.; Porter, M.; McIntosh, J. R. The Molecular Architecture of Axonemes Revealed by Cryoelectron Tomography. *Science* **2006**, *313*, 944−948.
(54) Bui, H.; Onodera, C.; Kidwell, C.; Tan, Y.; Graugnard, E.; Kuang, W.; Lee, J.; Knowlton, W.; Yurke, B.; Hughes, W. Programmable Periodicity of Quantum Dot Arrays with DNA Origami Nanotubes. *Nano Lett.* **2010**, *10*, 3367−3372.
(55) Pal, S.; Deng, Z.; Ding, B.; Yan, H.; Liu, Y. DNA-Origami-Directed Self-Assembly of Discrete Silver-Nanoparticle Architectures. *Angew. Chem., Int. Ed.* **2010**, *49*, 2700−2704.
(56) Tan, S.; Campolongo, M.; Luo, D.; Cheng, W. Building Plasmonic Nanostructures with DNA. *Nat. Nanotechnol.* **2011**, *6*, 268−276.
(57) Stephanopoulos, N.; Freeman, R.; North, H.; Sur, S.; Jeong, S.; Tantakitti, F.; Kessler, J.; Stupp, S. Bioactive DNA-Peptide Nanotubes Enhance the Differentiation of Neural Stem Cells into Neurons. *Nano Lett.* **2015**, *15*, 603−609.
(58) Aldaye, F.; Senapedis, W.; Silver, P.; Way, J. A Structurally Tunable DNA-Based Extracellular Matrix. *J. Am. Chem. Soc.* **2010**, *132*, 14727−14729.
(59) Hinds, B.; Chopra, N.; Rantell, T.; Andrews, R.; Gavalas, V.; Bachas, L. Aligned Multiwalled Carbon Nanotube Membranes. *Science* **2004**, *303* (5854), 62−65.
(60) Wang, H.; Zhou, W.; Yin, X.; Zhuang, Z.; Yang, H.; Wang, X. Template Synthesized Molecularly Imprinted Polymer Nanotube Membranes for Chemical Separations. *J. Am. Chem. Soc.* **2006**, *128*, 15954−15955.


DOI: 10.1021/acsnano.6b08008
*ACS Nano* XXXX, XXX, XXX−XXX

(61) Schulman, R.; Yurke, B.; Winfree, E. Robust Self-Replication of Combinatorial Information *via* Crystal Growth and Scission. *Proc. Natl. Acad. Sci. U. S. A.* **2012**, *109*, 6405−6410.
(62) Hariadi, R. F.; Yurke, B. Elongation-Flow-Induced Scission of DNA Nanotubes in Laminar Flow. *Phys. Rev. E* **2010**, *82*, 46307.
(63) Wickham, S.; Bath, J.; Katsuda, Y.; Endo, M.; Hidaka, K.; Sugiyama, H.; Turberfield, A. A DNA-Based Molecular Motor that Can Navigate a Network of Tracks. *Nat. Nanotechnol.* **2012**, *7*, 169−173.
(64) Mohammed, A. M.; Velazquez, L.; Chisenhall, A.; Schiffels, D.; Fygenson, D. K.; Schulman, R. Self-Assembly of Precisely Defined DNA Nanotube Superstructures Using DNA Origami Seeds. *Nanoscale* **2017**, *9*, 522−526.



DOI: 10.1021/acsnano.6b08008
*ACS Nano* XXXX, XXX, XXX−XXX